JOURNAL OF GEOPHYSICAL RESEARCH, VOL. 101, NO. C7, PAGES 16,615–16,629, JULY 15, 1996

An improved algorithm for the retrieval of ocean wave spectra from synthetic aperture radar image spectra

S. Hasselmann
Max-Planck-Institut für Meteorologie, Hamburg, Germany

C. Brüning[1]
Institut für Meereskunde, Universität Hamburg, Hamburg, Germany

K. Hasselmann and P. Heimbach
Max-Planck-Institut für Meteorologie, Hamburg, Germany

Abstract. An earlier algorithm for retrieving two-dimensional wave spectra from synthetic aperture radar (SAR) image spectra is improved by using a modified cost function and introducing an additional iteration loop in which the first-guess input spectrum is systematically updated. For this purpose a spectral partitioning scheme is applied in which the spectrum is decomposed into a finite number of distinct wave systems. At each iteration step, the individual wave systems of the partitioned nth-guess wave spectrum are adjusted to agree in mean energy, frequency, and direction with the corresponding mean values of the associated wave systems of the SAR-inverted wave spectrum. The algorithm retrieves smooth wave spectra, avoiding the discontinuities which tended to arise in the previous algorithm in the transition region near the azimuthal wavenumber cutoff of the SAR image spectrum. The azimuthal cutoff of the SAR spectrum is also reproduced more accurately. The greatest improvement of the new retrieval algorithm is obtained when the discrepancies between the initial first-guess wave spectrum and the observed SAR spectrum are large. In this case the additional updating loop for the input spectrum enables the retrieved spectrum to adjust such that the simulated SAR spectrum matches more closely the observed SAR spectrum. The overall correlation of a large set of simulated SAR spectra with the measured SAR spectra is found to be significantly higher than with the previous algorithm, indicating that the algorithm not only overcomes isolated shortcomings of the earlier algorithm but also yields retrieved wave spectra which are generally more consistent with the input SAR data. An additional practical advantage of the new algorithm is that it returns spectral partioning parameters which can be used in SAR wave data assimilation schemes.

1. Introduction

For many years, the possibility of quantitative measurements of ocean waves with a synthetic aperture radar (SAR) was seriously questioned. It was doubted whether the nonlinear distortions induced in the imaging process by the Doppler effects of the long-wave orbital velocities could be properly described. Nevertheless, the SAR imaging of ocean waves is now well understood (compare review by *Hasselmann et al.* [1985]), and the imaging theory has been successfully applied to compute SAR image spectra from wave spectra using Monte Carlo techniques [e.g. *Brüning et al.*, 1990] or, more recently, a closed spectral integral transform relation [*Hasselmann and Hasselmann*, 1991] (referred to in the following as HH), [*Krogstad*, 1992; *Hasselmann et al.*, 1994a; *Bao et al.*, 1994]. The forward mapping theory has been extensively verified against data from SEASAT, the Shuttle Imaging Radar-B (SIR-B) and the First European Remote Sensing satellite (ERS-1)

[1]Now at European Commission, Directorate-General for Science, Research and Development, Brussels, Belgium.

Paper number 96JC00798.
0148-0227/96/96JC-00798$09.00

[*Hasselmann et al.*, 1988, 1991; *Alpers et al.*, 1986; *Brüning et al.*, 1988; *Brüning et al.*, 1992, 1993; *Bao et al.*, 1994; *Hasselmann et al.*, 1994a; *Hansen et al.*, 1994; *Wilde et al.*, 1994] and in various field experiments such as the Labrador Extreme Waves Experiment (LEWEX) [*Beal*, 1991] and the Synthetic Aperture Radar and X-Band Ocean Nonlinearities - Forschungsplatform Nordsee (SAXON-FPN) [*Plant and Alpers*, 1994].

More difficult is the problem of inverting the nonlinear mapping relation to retrieve wave spectra from SAR image spectra. All frozen-image data suffer from an unavoidable 180° wave propagation ambiguity. In addition, because of the orbital wave motion effects, the SAR image spectrum is nonlinearly distorted and contains no information beyond a (sea-state dependent) azimuthal cutoff wavenumber. It follows that wave spectra can be meaningfully retrieved from SAR image spectra only if a first-guess wave spectrum from a model (or some other source) is available to resolve the ambiguities and supply the missing information beyond the cutoff.

In the following we shall assume, as in previous inversion algorithms, that both the forward mapping problem and the technical task of obtaining a calibrated SAR image of the sea surface from a satellite, for example, ERS-1/2, have been resolved. Thus if the SAR spectrum computed from a predicted wave spectrum disagrees with the measured SAR spectrum, we conclude that the predicted input wave spectrum must be incorrect. Conversely, if the input wave spectrum can be adjusted to yield a simulated SAR spectrum which agrees exactly with the observed SAR spectrum, we have extracted all the information from the observed SAR spectrum which is possible; we have solved the retrieval problem.

In practice, of course, neither the forward mapping relation nor the SAR image spectrum is free of errors. For example, although the forward mapping relation is dominated for typical satellite SAR incidence angles by the velocity bunching mechanism, which can be computed exactly, it depends to a lesser extent also on the hydrodynamic modulation transfer function, which is poorly known. Similarly, SAR image spectra depend on antenna gain properties which are not always calibrated perfectly. However, these problems are essentially independent of the problem of devising an effective retrieval algorithm. If a retrieval algorithm has been constructed for which the SAR spectrum computed from the retrieved wave spectrum agrees exactly with the SAR spectrum, but the assumed modulation transfer functions or SAR calibration factors are incorrect, the retrieved wave spectrum will, of course, be incorrect. However, once these errors are corrected, the identical retrieval algorithm will return correct wave spectra. Thus to demonstrate the quality of a retrieval algorithm, it is sufficient to show that the SAR spectrum computed from the retrieved wave spectrum agrees with the observed SAR spectrum. In the course of an overall system analysis one must investigate also other sources of error, but the retrieval problem as such may be regarded as resolved. Previous investigations cited above suggest that in the case of ERS-1 the other errors are small.

The standard technique for inverting nonlinear transform relations is to minimize a cost function which in the present case would penalize simultaneously both the errors between the first-guess and retrieved wave spectra and the deviations between the observed and simulated SAR spectra. Since the forward mapping relation is a complicated nonlinear integral, the retrieval algorithm involves an iterative loop in which the wave spectrum is successively adjusted to reduce the cost function (HH); [*Engen et al.*, 1994]. Through the derivation of a closed spectral integral transform relation which could be rapidly computed using Fast Fourier Transforms (HH), the application of such inversion algorithms has become operationally feasible [*Brüning et al.*, 1993, 1994a; *Hasselmann et al.*, 1994 a,b,c].

The inversion technique has been applied to the newly available global ERS-1 SAR wave-mode spectral data, which are computed and delivered in near real time from 10 km × 5 km imagettes every 200 km along the satellite track. The first-guess wave spectra required as input were obtained from the third-generation WAve Model (WAM) [*Wave Model Development and Implementation (WAMDI) Group*, 1988] which runs operationally at the European Centre for Medium Range Weather Forecasts (ECMWF, Reading, England). An important feature of these retrievals is that the wave spectrum can be calibrated independently of the SAR calibration using the approximately white-noise clutter background of the observed SAR image spectrum [*Alpers and Hasselmann*, 1982; *Brüning et al.*, 1994a,b].

The overall agreement between the first-guess and retrieved wave spectra in these analyses was very encouraging. A still closer agreement was found between the observed SAR image spectra and the simulated SAR spectra (computed from the retrieved wave spectra), indicating that the retrieval was generally working satisfactorily.

However, discrepancies were occasionally found in wave spectral intercomparisons, particularly in low-frequency swell systems, suggesting room for improvement. Assuming that the errors lie in the model first guess rather than in the SAR measurements and that the WAM model adequately simulates the wave physics, as verified in a number of studies [*WAMDI Group*, 1988; *Komen et al*, 1994], the most likely origin of the errors is the wind field. Waves respond very sensitively to the wind, the wave height being approximately proportional to the square of the wind speed, and the errors, once imprinted, can persist for long periods. Thus the impact of wind errors can clearly be seen in swell systems at long distances from their source. Wind field errors are found most frequently in the South Pacific, where analyzed winds are often underestimated because

of the sparseness of data. The identification of such errors through SAR wave mode measurements points to the considerable potential of a combined wind and wave data assimilation scheme, based on conventional and satellite data, for improved wave and weather forecasts [*Hasselmann et al.*, 1994c; *Bauer et al.*, 1994; S. Hasselmann et al., An optimal interpolation assimilation scheme for spectral wave data, submitted to *Journal of Geophysical Research*, 1996 (hereinafter referred to as Hasselmann et al., submitted manuscript, 1996)].

Intercomparisons between observed and simulated SAR spectra also reveal, however, occasional deficiencies in the retrieval algorithm as such. In this paper we remedy these problems, while at the same time retrieving wave spectral information in a form which can be readily applied in wave data assimilation schemes. The principal shortcomings and remedies are the following:

1. The azimuthal cutoff wavenumbers of the simulated SAR spectra are occasionally too low. This is usually accompanied by an overestimate of the retrieved spectral peak energy. As a remedy a new term is introduced into the cost function which penalizes errors in the cutoff wavenumber directly and readjusts the energy level of the entire wave spectrum accordingly (section 2). This affects also the energy level in the high-frequency part of the spectrum beyond the azimuthal cutoff. Although this part of the spectrum is not measured directly by the SAR, it has a strong influence on the SAR cutoff through its relatively large contribution to the rms orbital velocity, which is inversely proportional to the azimuthal cutoff wavenumber.

2. The retrieved wave spectra are occasionally more sharply peaked than the first-guess spectra. We attribute this to the fact that the global fast delivery spectral products provided by the European Space Agency (ESA) are smoothed to a 12×12 wavenumber directional grid. We therefore smooth and interpolate the SAR spectra computed from the wave spectra in the same way as the ESA fast delivery spectra at each iteration step of the cost function minimization scheme. This results both in a closer agreement of the observed and simulated SAR spectra and in more realistic looking wave spectra (section 2).

3. A discontinuity sometimes appears in the retrieved wave spectra in the neighborhood of the azimuthal cutoff wavenumber. This region separates the low wavenumbers for which SAR information was available from the higher wavenumbers without SAR information, where the retrieval algorithm automatically returns the first-guess spectrum. It was already shown in HH that a better agreement between observed and simulated SAR spectra could be achieved by pre-adjusting of the mean wave frequency and direction of the first-guess spectrum through a frequency re-scaling and rotation of the spectrum, prior to the application of the detailed inversion algorithm. However, this technique is applicable only for wave spectra containing a single wave system. We present here a generalization of the method to a superposition of different wave systems. To apply the general technique, we first decompose the wave spectrum into a number of different wave systems, using a modification of Gerling's (1992) spectral partitioning scheme [cf. *Brüning et al.*, 1994a; *Hasselmann et al.*, 1994 a,b]. We then adjust the different wave systems of the first-guess spectrum individually to the corresponding wave systems of the SAR-inverted wave spectrum. This is performed for each individual partitioned wave system by a rotation and rescaling of the frequency and energy scales.

In some cases the assignment between first-guess and SAR inverted wave systems cannot be made one to one. In these cases, first-guess wave systems are left unchanged if not observed by the SAR, while wave systems observed by the SAR but not present in the first-guess systems are simply added.

The reconstructed wave spectrum composed of the individually adjusted wave systems is then used as a new first guess, and the inversion procedure is repeated, if necessary, several times. The adjustment of the wave spectrum via the individual wave systems removes the discontinuity at the azimuthal cutoff wavenumber, while the additional iteration loop allows the input wave spectrum to depart further from the original first guess, leading to a closer agreement between the observed and final simulated SAR image spectrum. Another advantage of this approach is that the parameters of the partitioned wave systems are obtained as output, providing a convenient reduced data set for use in wave data assimilation schemes (section 3).

The results (section 4) show a marked improvement in the agreement between the simulated and observed SAR spectra. The algorithm is only weakly dependent on the first-guess spectrum, which is needed only to remove the 180° angular ambiguity and to provide information on the spectrum beyond the azimuthal cutoff. The wave spectra retrieved with the modified algorithm appear realistic at all wavenumbers. The retrieved spectra generally still show good agreement with the model first guess. However, in cases in which the first guess is not consistent with the observed SAR spectrum, the retrieved wave spectrum now deviates more strongly from the first guess than with the previous algorithm. This is due to the additional iteration loop in the retrieval algorithm, which decouples the retrieved spectrum from the first guess, enabling the simulated SAR spectrum to approach the observed SAR spectrum more closely. This is achieved, of course, at the "expense" of a larger departure of the retrieved wave spectrum from the first guess.

2. An Improved SAR Inversion Scheme

Theory

The mapping $P(\mathbf{k}) = \Phi(F(\mathbf{k}))$ of an ocean wave spectrum $F(\mathbf{k})$ into a SAR image spectrum $P(\mathbf{k})$ is given by a closed integral transform, which may be written as

a series expansion in the form (HH)

$$P(\mathbf{k}) = \exp(-k_x^2 \xi'^2) \sum_{n=1}^{\infty} \sum_{m=2n-2}^{2n} (k_x \beta)^m P_{nm}(\mathbf{k}), \quad (1)$$

where k_x denotes the wavenumber component of the long waves in the azimuthal direction, β is the ratio of the slant range to the platform velocity, and the spectral factors P_{nm} consist of Fourier transforms of higher-order products of the autovariance and covariance functions of the radial orbital velocity and the (real aperture radar) cross section modulation function. The index n indicates the nonlinearity order with respect to the input wave spectrum and the index m the order with respect to the velocity bunching parameter β. The (nonlinear) exponential factor depends on the mean square azimuthal displacement ξ'^2 of a scattering element

$$\xi'^2 = \beta^2 < u_r^2 >= \beta^2 \int |T_k^v|^2 F(\mathbf{k}) d\mathbf{k} \quad (2)$$

where $< .. >$ denotes the ensemble average and u_r the radial component of the orbital velocity of the ocean waves (cf. *Beal et al.*, 1983; *Alpers and Brüning*, 1986). The range-velocity transfer function T_k^v is given, according to classical surface wave theory, by

$$T_k^v = -\omega(\sin\theta \frac{k_y}{|k|} + i\cos\theta) \quad (3)$$

where ω denotes the radian frequency of the long waves, θ the incidence angle, and k_y the wavenumber component of the long waves in the range direction. Equation (1) can be rapidly evaluated by Fast Fourier Transforms, enabling the forward mapping relation to be inverted by iterative methods.

Extension of the Cost Function

We apply the standard technique of minimization of a suitably defined cost function, (HH), [*Brüning et al.*, 1994a,b; *Hasselmann et al.*, 1994a,b,c]. The cost function used by these authors contained two error terms: the deviation between the simulated and the observed SAR spectrum and a second term penalizing the deviation between the first-guess and retrieved wave spectrum. The second "regularization" term is needed to resolve the 180° angular ambiguity of the observed frozen-image SAR spectrum and to provide the missing information at high wavenumbers beyond the azimuthal cutoff of the SAR.

To remedy the first problem mentioned above, the occasional inaccurate simulation of the observed SAR cutoff, we extend the cost function of HH by including an additional term penalizing directly the deviation between the observed and simulated cutoff. For this purpose we define a clutter cutoff length scale as follows: First, a mean one-dimensional azimuthal SAR spectrum is computed by averaging over the range bins. To reduce the noise contribution, the range-bin averaging is restricted to the seven range bins bracketing the range bin of the spectral peak. The azimuthal cutoff length scale λ_{cl} is then defined as the wave length at which the mean azimuthal SAR spectrum has decreased to a value 3 dB above the noise floor.

To correct for errors in the cutoff, we introduce now a free energy-scaling parameter α. By applying the energy-scaling factor to the entire spectrum, rather than only to the low-wavenumber part of the spectrum for which SAR information is directly available, the factor α modifies also the high-wavenumber components beyond the azimuthal cutoff. These contribute significantly to the rms orbital velocity, which directly affects the rms azimuthal displacement ξ' (equation (2)) and thereby the cutoff length scale λ_{cl}. Assuming that ξ' and λ_{cl} are proportional, application of the energy scaling factor α leads to a modification $\lambda_{cl} \rightarrow \sqrt{(\alpha)}\lambda_{cl}$ of the simulated cutoff length scale.

In order to automatically adjust the scaling factor α so that the error between the observed and simulated cutoff is small, we thus add a cutoff error term to the cost function which now takes the form

$$J = \int [P(\mathbf{k}) - \hat{P}(\mathbf{k})]^2 \hat{P}(\mathbf{k}) d\mathbf{k} + \mu \int \frac{[F(\mathbf{k}) - \hat{F}(\mathbf{k})]^2}{\{B + \min[F(\mathbf{k}), \hat{F}(\mathbf{k})]\}^2} d\mathbf{k} + \eta \frac{(\alpha\lambda_{cl}^2 - \hat{\lambda}_{cl}^2)^2}{\max\{\lambda_{cl}^4, \hat{\lambda}_{cl}^4\}} \quad (4)$$

where $\hat{F}(\mathbf{k})$ denotes the first-guess wave spectrum, $\hat{P}(\mathbf{k})$ the observed SAR spectrum, and $P(\mathbf{k})$ the SAR spectrum computed from the best-fit wave spectrum $F(\mathbf{k})$ and $\hat{\lambda}_{cl}$, λ_{cl} denote the clutter cutoff length scales of the observed and simulated SAR image spectra, respectively. The weighting factor μ is chosen to be sufficiently small ($\mu = 10^{-3}\hat{P}_{\max}^3$) so that the form of the first-guess wave spectrum $\hat{F}(\mathbf{k})$ has only a small impact on the final solution where SAR information is available but is still large enough to resolve the 180° directional ambiguity and determine the form of the high wavenumber part of the spectrum beyond the SAR azimuthal wavenumber cutoff. The weight $\eta = 0.5 \times 10^5 [\int \hat{P}(\mathbf{k}) d\mathbf{k}]^3$ is chosen such that the first and third terms of (4) are of the same order of magnitude. A small constant $B(= 10^{-4}\hat{F}_{\max})$ is introduced to prevent the denominator of the second term from vanishing.

The extended cost function **J** yields a better agreement of the simulated and observed cutoff through direct modification of the total energy of the wave spectrum. It also generally leads to a smoother transition of the retrieved wave spectrum across the cutoff wavenumber separating the low-wavenumber region which is modified by SAR spectral data from the high-wavenumber tail where no SAR information is available.

Modification of the Numerical Inversion Scheme

The iteration scheme used by HH to minimize the cost function proceeded as follows: Start from a first-guess wave spectrum $F^1(\mathbf{k}) = \hat{F}(\mathbf{k})$ and associated SAR spec-

trum $P^1(\mathbf{k})$, computed from $F^1(\mathbf{k})$ using the fully nonlinear mapping relation. Assume that at the beginning of the nth iteration step a wave spectrum $F^n(\mathbf{k}) = F^n$ and its associated SAR spectrum $P^n(\mathbf{k}) = \Phi(F^n) = P^n$ have been determined. An improved estimate of the wave spectrum

$$F^{n+1} = F^n + \triangle F^n \tag{5}$$

with associated estimate

$$P^{n+1} = \Phi(F^{n+1}) \tag{6}$$

of the SAR spectrum is then constructed in two stages.

First, it is assumed that an approximation δP^n of the SAR spectral increment $\triangle P^n = P^{n+1} - P^n$ can be computed from $\triangle F^n$ using the quasi-linear SAR-wave spectral mapping relation

$$P(\mathbf{k}) \sim \exp\,(-k_x^2 \xi'^2) P_1(\mathbf{k}) \tag{7}$$

which is given by the truncation of (1) at the nonlinearity index $n = 1$,

$$\begin{aligned} P_1(\mathbf{k}) &= \sum_{m=0}^{2} (k_x \beta)^m P_{1m}(\mathbf{k}) \\ &= |T_{\mathrm{SAR}}(\mathbf{k})|^2 F(\mathbf{k}) + |T_{\mathrm{SAR}}(-\mathbf{k})|^2 F(-\mathbf{k}) \end{aligned} \tag{8}$$

where $T_{\mathrm{SAR}}(\mathbf{k})$ represents the transfer function of the standard linear SAR image mapping relation [cf. *Hasselmann et al.*, 1985], (HH). Thus we set

$$\delta P^n = W_{\mathbf{k}} \triangle F^n(\mathbf{k}) + W_{-\mathbf{k}} \triangle F^n(-\mathbf{k}) \tag{9}$$

where

$$W_{\mathbf{k}} = |T_{\mathrm{SAR}}(\mathbf{k})|^2 \exp\,(-k_x^2 \xi^{n'2}) \tag{10}$$

Since the relation between δP^n and $\triangle F^n$ is linear (the factor $\exp\,(-k_x^2 \xi'^2)$ in (7) is regarded as known from the previous interation step), substitution of these changes into the cost function yields a soluble quadratic minimization problem for $\triangle F^n$.

Having determined $\triangle F^n$ and thus F^{n+1}, P^{n+1} is computed in the second stage of the iteration step by applying the full nonlinear mapping relation to F^{n+1}. The iteration is then repeated.

To include now adjustments of the energy scale α, we modify the iteration method by setting

$$F^{n+1} = \alpha^n F^n + \triangle F^n, \tag{11}$$

where α^n is computed after $\triangle F^n$ has been determined by the above method (note that n denotes here an index, not an exponent). Thus we compute again an approximation δP^n of $\triangle P^n$ from $\triangle F^n$ using (9). Substituting (11) into (4), setting $P^{n+1} \simeq P^n + \delta P^n$, and defining, for brevity, $\mu^n = \mu[B + \min\{F^n, \hat{F}\}]^{-2}$ and $\eta^n = \eta \left[\max(\lambda_{cl}^4, \hat{\lambda}_{cl}^4)\right]^{-1}$, the cost function, expressed in terms of $\triangle F^n$ and δP^n, then becomes

$$\begin{aligned} J &= \int \hat{P}[\delta P^n - (\hat{P} - P^n)]^2 d\mathbf{k} + \\ &\quad \int \mu^n [\triangle F^n - (\hat{F} - \alpha^n F^n)]^2 d\mathbf{k} + \\ &\quad \eta^n (\alpha^n \lambda_{cl}^{n2} - \hat{\lambda}_{cl}^2)^2 \end{aligned} \tag{12}$$

The linearized variational problem

$$\delta J / \delta \triangle F^n(\mathbf{k}) = 0 \tag{13}$$

and

$$\delta J / \delta \alpha = 0 \tag{14}$$

is solved first with respect to $\triangle F^n$ for fixed α^n, which is taken as the value determined from the last iteration step, $\alpha^n = \alpha^{n-1}$ (with $\alpha^1 = 1$). This yields (compare HH)

$$\begin{aligned} \triangle F_{\mathbf{k}}^n &= \frac{A_{-\mathbf{k}}[W_{\mathbf{k}} \triangle \hat{P}_{\mathbf{k}}^n + \mu^n \triangle \hat{F}_{\mathbf{k}}^n]}{A_{\mathbf{k}} A_{-\mathbf{k}} - B_{\mathbf{k}}{}^2} - \\ &\quad \frac{B_{\mathbf{k}}[W_{-\mathbf{k}} \triangle \hat{P}_{\mathbf{k}}^n + \mu^n \triangle \hat{F}_{-\mathbf{k}}^n]}{A_{\mathbf{k}} A_{-\mathbf{k}} - B_{\mathbf{k}}{}^2} \end{aligned} \tag{15}$$

where

$$\triangle \hat{P}_{\mathbf{k}}^n = \hat{P}(\mathbf{k}) - P^n(\mathbf{k}) = \hat{P}(-\mathbf{k}) - P^n(-\mathbf{k}) \tag{16}$$

$$\triangle \hat{F}_{\mathbf{k}}^n = \hat{F}(\mathbf{k}) - \alpha^n F^n(\mathbf{k}) \tag{17}$$

$$A_{\mathbf{k}} = W_{\mathbf{k}}{}^2 + 2\mu^n \tag{18}$$

and

$$B_{\mathbf{k}} = W_{\mathbf{k}} W_{-\mathbf{k}} \tag{19}$$

Subsequently, the energy scaling parameter α^n is obtained by solving (14):

$$\alpha^n = \frac{\eta^n \hat{\lambda}_{cl}^2 \lambda_{cl}{}^n 2 - \mu^n \int F_{\mathbf{k}}^n [\triangle F_{\mathbf{k}}^n - \hat{F}_{\mathbf{k}}] d\mathbf{k}}{\eta^n \lambda_{cl}{}^{n4} + \mu^n \int F_{\mathbf{k}}^{n2} d\mathbf{k}} \tag{20}$$

Equations (15) and (20) are solved iteratively. First, (15) is solved using α^{n-1}, yielding an approximation for $\triangle F_{\mathbf{k}}^n$, which is then used to solve (20), yielding an approximation for α^n, which again is then used to solve (15), etc. The iteration ends when α^n changes less than 1%.

Having determined $\triangle F_{\mathbf{k}}^n$ and α^n and thus F^{n+1}, the associated SAR spectrum P^{n+1} is again computed from F^{n+1} using the full nonlinear SAR transformation relation, and the iteration is repeated. To maintain numerical stability, it was found necessary to restrict $\triangle F_{\mathbf{k}}^n$ to the range $|\triangle F_{\mathbf{k}}^n| \leq \min[\hat{F}_{\mathbf{k}}^n, \alpha F_{\mathbf{k}}^n]/4$ if

$$\frac{\mu \triangle F_{\mathbf{k}}^{n2}}{B + \min[F(\mathbf{k}), \hat{F}(\mathbf{k})]^2} \geq 0.25[P^n(\mathbf{k}) - \hat{P}(\mathbf{k})]^2 \hat{P}(\mathbf{k}) \tag{21}$$

The iteration generally converges after 6-10 iteration steps (as in the original method of HH). If the azimuthal

clutter cutoff length scale is not well defined (for SAR spectra with a low signal-to-noise ratio), we reduce (12) to the original form (4) by setting $\alpha = 1$ and $\eta = 0$.

Matching the Interpolation Schemes of the Observed and Computed SAR Spectra

The second problem mentioned above, the occasional retrieval of too sharply peaked wave spectra, was resolved by introducing an additional smoothing filter into the computation of the SAR spectra from the wave spectra. This made the inversion algorithm more consistent with the smoothing interpolation used in the generation of the ESA fast delivery product. A proper matching of the filters of the computed and observed SAR spectra is needed also to correctly reproduce the azimuthal cutoff, which is particularly sensitive to the form of smoothing.

The inversions are performed on a 128 x 128 wavenumber grid with a Nyquist wavenumber $k_x^{\mathrm{Nyq}} = k_y^{\mathrm{Nyq}} = 2\pi/32m^{-1}$. To carry out the inversions, the ERS-1 fast delivery imagette spectra, which are given on a coarse polar coordinate grid (12 wavenumbers, 12 directions between 0° and 180°) are transformed from polar to cartesian (k_x, k_y) coordinates. The SAR terms in the cost function are evaluated only in the domain for which reliable SAR data were available, i.e., in the ring $(2\pi/800)\ \mathrm{m}^{-1} \leq |\mathbf{k}| \leq (2\pi/100)\ \mathrm{m}^{-1}$. The coarse resolution of the ERS-1 SAR wave mode product causes a smearing and broadening of the retrieved SAR image spectra, affecting in particular the estimate of the azimuthal clutter cutoff length scale. To avoid unrealistic changes of the total wave energy induced by the new cutoff term in the cost function due to this artificial spectral broadening (and to achieve also some smoothing across the azimuthal cutoff region), the SAR spectra computed from the model spectra were treated in the same way as the ESA spectra: they were first transformed from the high-resolution cartesian (k_x, k_y) grid to the ESA low-resolution polar (k, ϕ) grid and then reinterpolated to the high-resolution cartesian (k_x, k_y) grid at each SAR spectrum computation in the inversion scheme (this can, of course, be expressed as a single net smoothing operation).

The above considerations apply for SAR spectra without clutter-noise contamination. In practice, the observed SAR spectrum consists of a superposition of the wave image spectrum and a background clutter spectrum. To first order, the two spectra are simply linearly superimposed, the modulation of the clutter noise by the ocean waves being negligible. The clutter spectrum can thus be removed by subtraction. Below the high wavenumber roll-off due to the system impulse response function, the clutter spectrum is essentially white [*Alpers and Hasselmann*, 1982; *Wilde et al.*, 1994]. It can be estimated from the background spectral level at wavenumbers slightly beyond the azimuthal cutoff. In this range the clutter spectrum is still essentially white, but the wave contribution is no longer present. The clutter level was estimated as the average of the five lowest spectral values of the highest wavenumber $(k = 2\pi/100m)$ bins of the SAR (fast delivery) spectral product. This value was subtracted from the SAR spectra prior to further processing. The clutter level was used also to calibrate the retrieved wave spectrum [cf. *Alpers and Hasselmann*, 1982; *Brüning et al.*, 1994a,b].

3. Iteration of the Input Wave Spectrum

In addition to the modifications of the inversion scheme discussed in the previous section, a further change in the present retrieval algorithm is the introduction of an iteration scheme for successively adapting the first-guess input wave spectrum to the previously retrieved wave spectrum. This resolves the third problem mentioned above: the occurence of discontinuities in the retrieved spectra in the neighborhood of the azimuthal cutoff wavenumber. It also yields an improved agreement between the simulated and observed SAR spectrum when the first guess is rather far from the observations. As pointed out above, a first-guess wave spectrum is needed for SAR wave spectral retrievals in order to overcome the 180° directional ambiguity and to provide the missing information beyond the azimuthal SAR cutoff. However, the introduction of a term penalizing deviations from the first-guess spectrum in the cost function tends to inhibit large departures of the retrieved spectrum from the first guess, thus preventing the retrieved spectrum from adjusting to the observed SAR spectrum if the first guess is poor.

It can be argued that this is a desirable feature which is regularly incorporated, for example, in data assimilation schemes. Since the first guess is also based on data (although filtered through a model), it should be given an appropriate weight relative to the additional data provided by the SAR. However, we adopt here the view that the weighting of different data sources, including the model first guess, should be assigned to a subsequent data assimilation operation and should not be folded into the retrieval process as such. The retrieval should attempt to extract the full information content of the SAR, using the first-guess data only to augment the incomplete information of the SAR, not to compete with the SAR data.

This is achieved through the introduction of an additional iteration loop which successively modifies the first-guess spectrum. At each iteration, the original information from the first guess is diluted at the cost of the new SAR information. Consequently, the only initial information which is retained asymptotically is information which is not contained in the SAR data.

The iterations yield second-guess, third-guess, etc., input spectra. We shall refer to these in the following as "input" wave spectra, as opposed to the original first-guess spectra. To distinguish the final retrieved spectra from the intermediate inversion products obtained in the course of the iteration of input spectra, we shall

refer to the final product as the "retrieved" spectra and the intermediate products as "inverted" spectra (a more precise definition of the intermediate "inverted" spectra will be given later in this section).

The iteration scheme makes use of two techniques which were mentioned briefly in the first section: a partitioning scheme for the decomposition of wave spectra into a small number of discrete wave systems and an algorithm for the cross assignment of the wave systems of different spectra.

The Wave Partitioning Scheme

Two-dimensional wave spectra observed in the open ocean normally consist of a complex superposition of waves from several generation areas. To reduce the large number of degrees of freedom of observed and modeled two-dimensional wave spectra to a manageable number of parameters, while still retaining the principal characteristics of the complex structures of real ocean wave spectra, Gerling [1992] devised a spectral partitioning scheme. We use in the following a modification of Gerling's scheme as applied by *Brüning et al.*, [1993], *Brüning et al.*, [1994a] and *Hasselmann et al.*, [1994c] for the analysis of ERS-1 SAR wave mode data. The scheme has been used also in a wave data assimilation method developed by S. Hasselmann et al., (submitted manuscript, 1996).

The wave partitioning method subdivides the two-dimensional wave spectrum into a number of separate superimposed wave systems, each of which can be characterized by a relatively small number of mean parameters, such as the significant wave height H_s, mean frequency $\overline{f}$, propagation direction $\overline{\theta}$, and directional spread $\overline{\delta f^2}$.

Following *Brüning et al.* [1994a,b], the wave systems are defined in term of inverted "catchment areas". A wave system consists of all spectral points whose "run-off" drains into a local (inverted) peak. Mathematically, the wave systems can be defined (and constructed) by a simple induction rule: each spectral grid point is assigned to the same wave system as its immediate steepest ascent neighbor. If a grid point has higher energy than all of its neighbors, the grid point represents a local peak and defines a wave system.

Formally separate wave systems are coalesced if they satisfy at least one of the following three conditions: (1) they lie too close to one another, namely their peaks are only one grid point apart, (2) the "valley" separating the peaks is not sufficiently low: minimum spectral value between two peaks is greater than 85 % of the smaller of the two peaks, or (3) the spectral spread $\overline{\delta f^2}$ of both systems is larger than the square distance $\Delta f^2 = (f_x^{(1)} - f_x^{(2)})^2 + (f_y^{(1)} - f_y^{(2)})^2$ between the two peaks $(f_x^{(1)}, f_y^{(1)}), (f_x^{(2)}, f_y^{(2)})$, where the spectral spread is defined as $\overline{\delta f^2} = \overline{(f_x - \bar{f}_x)^2} + \overline{(f_y - \bar{f}_y)^2}$ with $\bar{f}_x = \overline{f \cos\theta}$, $\bar{f}_y = \overline{f \sin\theta}$ and the overbar denotes usual averages weighted with the spectral density.

For applications in general wave data assimilation schemes in which not only the wave field but also the wave-generating wind field is updated, a classification of wave systems into wind sea, old wind sea, swell, and mixed wind sea-swell is useful. Although not needed for the retrieval algorithm, we describe briefly the classification scheme used here in view of the direct application of the extended retrieval algorithm for wave data assimilation.

A wave system is classed as wind sea if the phase velocity at the spectral peak is less than 1.3 times the component of the wind speed in the wave propagation direction. Old wind seas are defined analogously, the ratio of the phase velocity to the wind speed component in the wave propagation direction lying in this case in the interval $1.3 - 2.0$. Mixed wind sea-swell systems occur in turning wind situations. If the change in wind direction is relatively slow, a new wind sea peak is not immediately built up in the new wind direction, since the nonlinear transfer couples the wave components developing in the new wind direction to the former wind sea propagating still in the old wind direction [cf. *Young et al.*, 1987]. This results in a skewed single-peaked spectrum containing both new wind sea components and old wind sea (swell), the peak being located still at the position of the old wind sea peak. The identification of such coupled wind sea-swell systems needs to be based on a criterion involving not simply the peak of the system but also the new waves developing in the turned wind direction. The following definition was found to be satisfactory: a mixed wind sea-swell system is a wave system for which the peak fails to satisfy the pure or old wind sea criterion, but one of the two spectral components $(\bar{f} + \delta f, \bar{\theta} \pm \delta\theta)$, where $\delta f^2 = \overline{\delta f^2}$, $\delta\theta^2 = \overline{\delta f^2}/\overline{f_p^2}$ does. Finally, wave systems which fall into none of the wind sea-related categories, are classed as swell.

Cross Assignment of Spectral Wave Systems

The adjustment of the input wave spectrum in the iterative retrieval algorithm is performed by modifying the wave systems of the input spectra. The characteristic parameters of the wave systems (significant wave height H_s, mean wave frequency $\bar{f}$, and mean direction $\bar{\theta}$) are adjusted to agree with the parameters of the corresponding wave systems of the inverted wave spectra. This requires first a criterion for cross assigning the wave systems of the input and inverted spectra. We chose an assignment algorithm based on the minimum normalized square distance D^2 in wavenumber space between appropriately defined characteristic wavenumber vectors (k_x^w, k_y^w) and (k_x^s, k_y^s) of the wave systems of the input and SAR inverted wave spectra, respectively, where

$$D^2 = \frac{(k_x^w - k_x^s)^2 + (k_y^w - k_y^s)^2}{(k_x^{w2} + k_x^{s2}) + (k_y^{w2} + k_y^{s2})} \tag{22}$$

The characteristic wavenumber vectors are defined as $k_x^{w/s} = k^{w/s} \cos\tilde{\theta}$ and $k_y^{w/s} = k^{w/s} \sin\tilde{\theta}$, where $k^{w/s} =$

$4g^{-1}\pi^2(\tilde{T}^{w/s})^{-2}$ and the tilde denotes the values which are modified relative to the usual spectral-weighted definition by the introduction of an additional factor $1/f$ to confer more weight to the low-frequency part of the spectrum which contains the relevant SAR information. Thus

$$\tilde{T} = \frac{\int\int F(f,\theta)\frac{T}{f}dfd\theta}{\int\int F(f,\theta)\frac{1}{f}dfd\theta} = \frac{\overline{T^2}}{\overline{T}} \tag{23}$$

Individual wave systems of the first-guess and SAR retrieved spectrum are cross assigned if their normalized squared distance is less than some critical value D^2_{crit}. Satisfactory results were achieved for the value $D^2_{\text{crit}} = 0.75$.

The inverted SAR spectrum occasionally contains more partitioned wave systems than the first-guess spectrum. This can be due to noise in the observed SAR spectra (the imagette spectra are based on relatively few degrees of freedom at low frequencies) or to discontinuities in the inverted spectra near the azimuthal cutoff separating the regions with and without SAR information. To remove artificial wave systems generated in this manner, two wave systems of the inverted SAR spectra are coalesced and cross assigned to a single input wave system if each of their normalized square distances to the input wave system is less than 0.75. If a wave system of an inverted SAR spectrum cannot be cross assigned to an input wave system, it is simply superimposed on the corrected input wave spectrum.

The SAR Retrieval Algorithm

The individual input wave systems are adjusted to the characteristic parameters of the cross assigned wave systems of the inverted SAR spectrum by a rotation and a rescaling of the frequency and energy axes. The corrected wave systems are then recombined by linear superposition to yield a corrected two-dimensional wave spectrum. Spectral grid points in which wave systems overlap after adjustment are averaged, while gaps between wave systems are filled by a two-dimensional parabolic fit. The resulting corrected spectrum is then used as input for the inversion in the next iteration step. The term "inverted" spectrum, introduced earlier to denote the intermediate wave spectra generated while iterating the input spectrum, will be used in the following to denote the wave spectra produced by the inversion algorithm, prior to the partitioning corrections used to update the input.

The impact of iterating the input spectrum is strongest when the retrieved spectrum deviates significantly from the model first guess. However, in this case, there is also a danger that the SAR data may be incorrect, leading to an unrealistic wave spectral retrieval. The development of an unrealistic retrieval is usually accompanied by a breakdown in convergence: after a few iteration steps during which the error between the simulated and observed SAR spectra decreases, the error begins to grow again. This is due to the adjustment of the input wave systems to the unrealistic wave systems of the inversion. The rescaled wave systems transmit the unrealistic features to higher wavenumbers, thereby affecting also the SAR cutoff and producing a poorer agreement with the observed SAR spectrum. To prevent a drift into an unrealistic retrieval, the iteration was therefore terminated when the dimensionless square error

$$\epsilon^2 = \frac{\int\int [S_s(f,\theta) - S_o(f,\theta)]^2 dfd\theta}{\sqrt{\int\int [S_s(f,\theta)]^2 dfd\theta \int\int [S_o(f,\theta)]^2 dfd\theta}} \tag{24}$$

between the simulated and observed two-dimensional SAR image specta S_s and S_o, respectively, was a minimum. (In practice, a fixed number of iterations, typically five, was carried out, and the iteration with the smallest error was then selected as the retrieval.)

4. Results

An example of a complex wave spectrum retrieved from the ERS-1 SAR wave mode spectrum is presented in Figure 1. Figure 1a shows the model first-guess wave spectrum. The wave spectrum derived by inversion using the first guess without iteration is shown in Figure 1b, and the final retrieval after five iterations of the input spectrum in Figure 1c. The wave systems of the final retrieved spectrum are seen to differ significantly from the wave systems of the first-guess spectrum, while the deviations for the wave spectrum obtained by direct inversion from the first-guess input spectrum are generally smaller.

The largest differences are seen in the southward propagating swell systems. The southwestward running system of the final retrieval is barely detectable in the first-guess spectrum (where it does not even show on the plot). However, good agreement is seen in the northeast propagating wind-wave system.

The retrieved spectra show small corrections in the high-frequency wind sea region of the spectrum beyond the azimuthal cutoff of the SAR. These are due to the adjustment of the overall energy level of the spectrum to reproduce the observed azimuthal cutoff, achieved through the additional cutoff error term in the cost function.

Figure 2 illustrates the improvement of the retrievals resulting from this error term. Figure 2a shows a first-guess wave spectrum, Figure 2b the wave spectrum derived from the first guess using the former retrieval algorithm of HH with no cutoff term in the cost function, Figure 2c shows the inversion using the scheme presented in this paper, applied again to the first-guess spectrum, and Figure 2d shows the retrieved wave spectrum using the full retrieval algorithm with iteration of the input wave spectrum. The simulated SAR spectrum from the inversion with the additional cutoff term (Figures 2g and 2h) shows a considerable improvement in

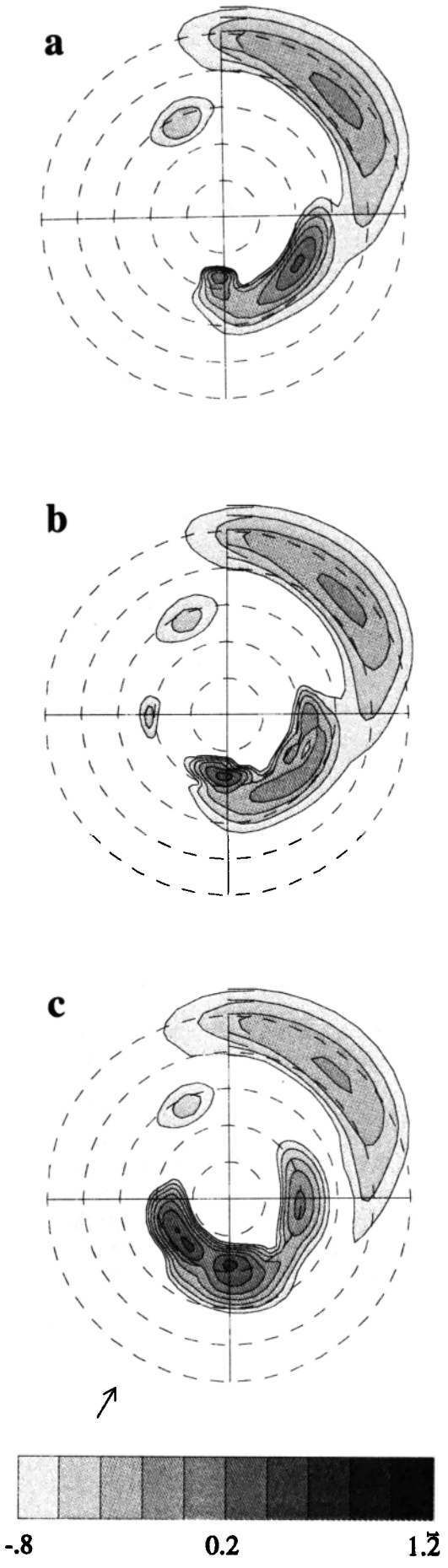

the azimuthal wavenumber cutoff relative to the first-guess case (Figure 2e) or the original HH retrieval (Figure 2f), and is in good agreement with the observed SAR spectrum (Figure 2i). To reproduce the observed cutoff wavenumber, the energy level of the retrieved wave spectrum is decreased in the present algorithm to 4.75 m significant wave height in the noniterated case and to 4.82 m in the full retrieval as compared with 6.2 m for the original HH algorithm.

The statistical improvement in the representation of the azimuthal cutoff achieved with the present inversion algorithm (without iteration of the input spectrum) is demonstrated in Figure 3 for a 1-day global data set. The scatter between the observed and the first-guess clutter cutoff is reduced significantly in the present inversion scheme.

The impact of the iteration of the input spectrum is illustrated more clearly for the two sets of wavenumber spectra shown in Figures 4a and 4b. The columns of each panel show the first and final inversion, and the rows show various wave and SAR spectra. The SAR spectra (first columns, second row) computed from the input wave spectra (first columns, first row) show little similarity with the observed SAR spectra (fifth row). However, the SAR spectra (first column, fourth row) computed from the wave spectra of the first inversion (first column, third row) already exhibit an adjustment of the spectral peaks to the observed peaks. The agreement between the simulated and observed SAR spectra (rows 4 and 5) is significantly improved for the minimal-error optimal retrievals (three iterations, Figure 4a, and four iterations, Figure 4b). The optimal retrieved wave spectra (row 6) exhibit significantly larger differences relative to the first-guess WAM spectra than the noniterated retrievals.

Besides the error defined in (24) we can also use the pattern correlation index as a measure of the agreement of the observed and simulated SAR spectra S_o, S_s (as given by *Brüning et al.* [1994]):

$$C = \frac{\int\int S_s(f,\theta) S_o(f,\theta) df d\theta}{[\int\int S_s^2(f,\theta) df d\theta \int\int S_o^2(f,\theta) df d\theta]^{\frac{1}{2}}} \qquad (25)$$

For the two cases shown in Figure 4, the pattern correlation of the SAR spectra computed from the first guess WAM spectrum and the observed SAR spectrum is 0.67

Figure 1. (a) First guess wave spectrum, (b) wave spectrum retrieved from the non-iterated first-guess wave spectrum according to the new inversion algorithm, (c)and wave spectrum retrieved by iteration of the input wave spectrum according to the present retrieval algorithm in polar frequency-directional plots. Circles denote frequencies at 0.05 Hz intervals starting at 0.05. Isolines are logarithmically spaced relative to the maximum value of the spectral energy density. The arrow denotes speed (13m/sec) and direction of the local wind

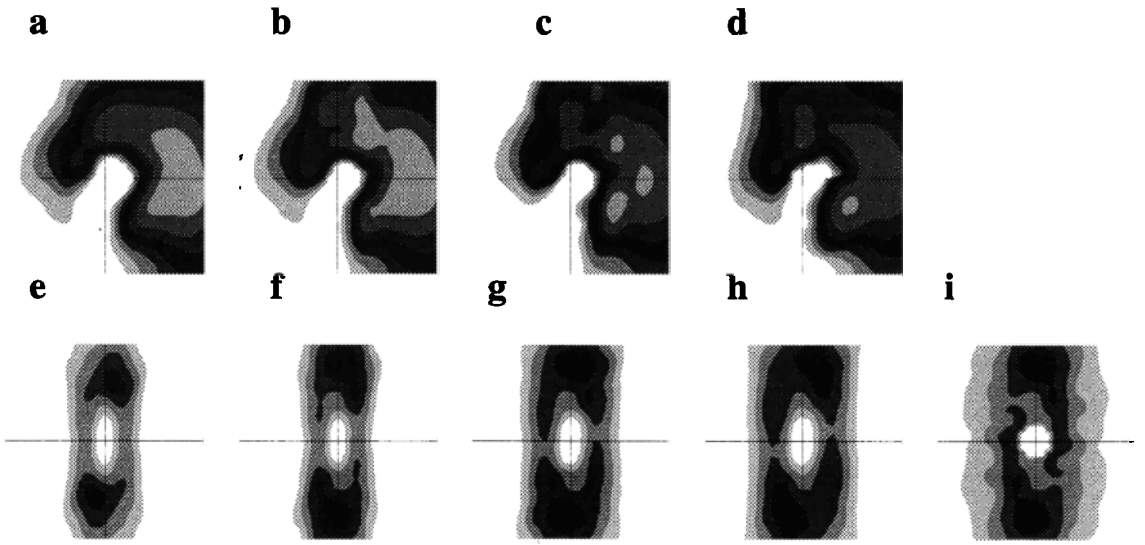

Figure 2. (a) First-guess wave spectrum, (b-c) spectrum retrieved from the non-iterated first-guess spectrum (former inversion algorithm, Figure 2b; present algorithm Figure 2c), (d) retrieved wave spectrum after iteration of the input spectrum (new algorithm, Figure 2d), (e - h) synthetic aperture radar (SAR) spectra computed from the wave spectra of Figure 2a - 2d, respectively, and (i) the observed SAR spectrum. Spectra are plotted in wavenumber space with $|k| < 100m$; k_x denotes the azimuthal direction.

for Figure 4a and 0.54 for panel Figure 4b. The pattern correlation indices for the optimal retrievals increased to 0.91 in both cases.

Contrary to this example, the first-guess wave spectra normally already show good agreement with the first inversions [cf. *Brüning et al.*, 1993, 1994a,b], and a high pattern correlation between the simulated and observed SAR spectra, typically above 0.9, is achieved without iteration. However, in cases in which the SAR indicates discrepancies in the model first-guess wave spectra, a significant improvement can be achieved by iterating the input spectrum. This is illustrated by the statistical data for 2729 retrievals for an 8-day period in March 1993 (Figure 5). When the initial error ϵ^2 (equation (24)) is large, it is significantly reduced by optimally iterating the input spectrum (Figure 5a).

Figure 5a and 5c show a further illustration of the improval of the present algorithm including an additional input-spectrum iteration loop over an algorithm without this feature, as used, for example, by *Brüning et al.* [1994a] in their first analysis of ERS-1 SAR wave mode data. The panels show a comparison of the distribution of the errors and the correlation indices between the simulated and observed SAR spectra for the same sample of data as used by *Brüning et al.* [1994a] for the original single inversion (but with a modified cost function, as described above) and the iterated full retrieval. The agreement between the observed and simulated SAR spectra is seen to be significantly improved compared with the original one-shot inversion method of HH. (As has been pointed out, the quality of a retrieval algorithm can be judged only by its ability to reproduce the observed SAR spectrum, independent of the question of the accuracy of the SAR modulation transfer function determining the forward transfer relation or the actual SAR measurement).

Ideally, the retrieved wave spectra obtained with the iterative algorithm should be only weakly dependent on the first-guess spectra. These should provide only the information needed to resolve the 180° angular ambiguity and to augment the spectra at high wavenumbers beyond the azimuthal cutoff. That this input information is needed is illustrated in Figure 6, in which the retrievals are compared for the case of a first-guess WAM spectrum (Figure 6a) and a Joint North Sea Wave Project (JONSWAP) spectrum [*Hasselmann et al.*, 1973] (Figure 6b). The JONSWAP spectrum shows only one wave system in range direction, while the first-guess model spectrum shows two range traveling wave systems. The optimal iterations (8 for Figure 6a and 16 for Figure 6b) show close agreement between the simulated and observed SAR spectra in both cases, with correlation indices of 0.94 (Figure 6a) and 0.98 (Figure 6b). However, the final retrieved spectra (last spectra, second columns) show low frequency swell systems running in opposite directions for the two cases. Swell energy was present in the first-guess WAM spectrum but not in the JONSWAP spectrum. Thus the 180° angular ambiguity could not be resolved for the first-guess JONSWAP spectrum.

Both cases also illustrate, through the generation of energy in the upper wavenumber half plane of the final retrieved wave spectrum, that the iteration of the input wave spectrum permits the retrieval to gradually drift

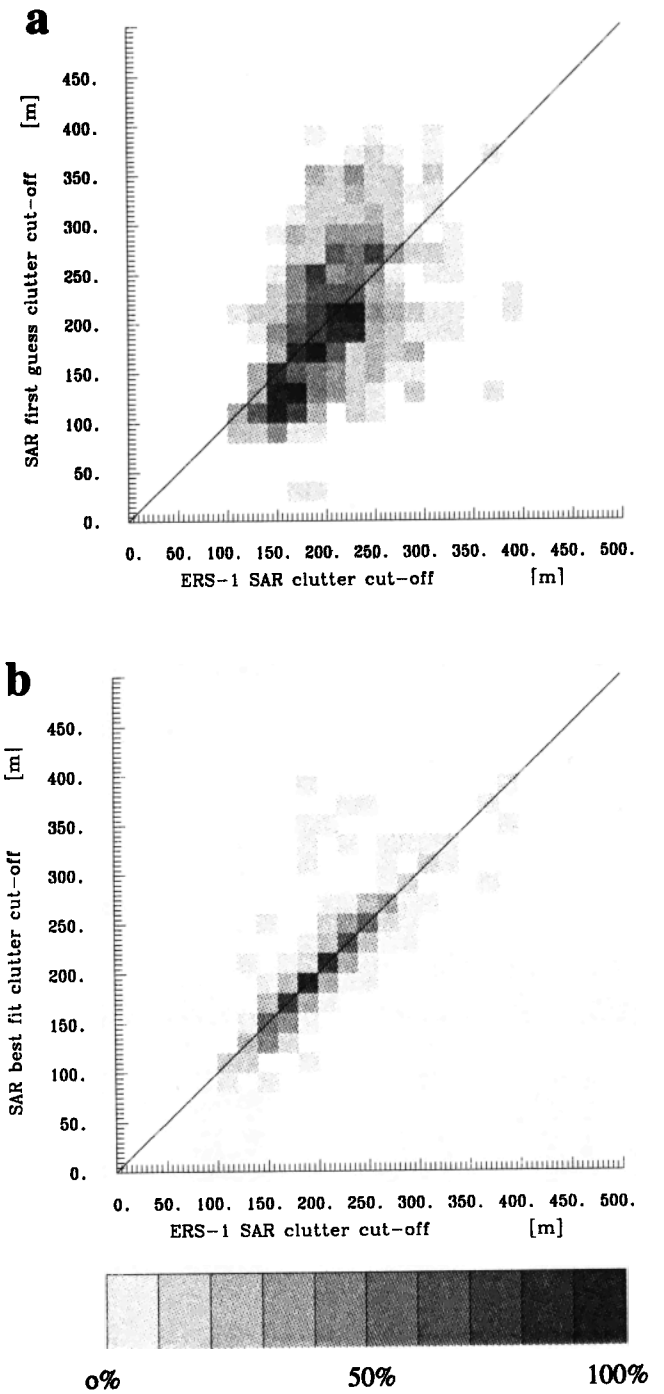

Figure 3. (a) Comparison of model-derived (first-guess) and observed clutter cutoff wavelengths for the global set of spectra obtained on November 25, 1992; (b) comparison of model-derived (best-fit) and observed clutter cutoff wavelengths for the global set of spectra obtained on November 25, 1992. Grey scale represents density classes of scatterdiagrams, beginning with the lowest density (dark grey pixels, summing to 10% of all cases).

away from the first-guess spectrum. In these examples, the improvement of the simulated SAR spectrum after a large number of iterations is marginal when compared with the retrieval after only a few iterations, while the change in the retrieved wave spectrum produced by the later iterations is appreciable. In such cases it may be advisable to modify the cost function by reinstating a small error term penalizing the deviation of the retrieval from the original first-guess wave spectrum.

In most cases, however, the ability of the present SAR retrieval algorithm to retrieve new wave systems which are inferred from the SAR but not present in the first-guess spectrum is a desirable feature. This is illustrated in Figure 7. The first guess-wave spectrum (Figure 7a) shows a pronounced mixed wind sea-swell system, with

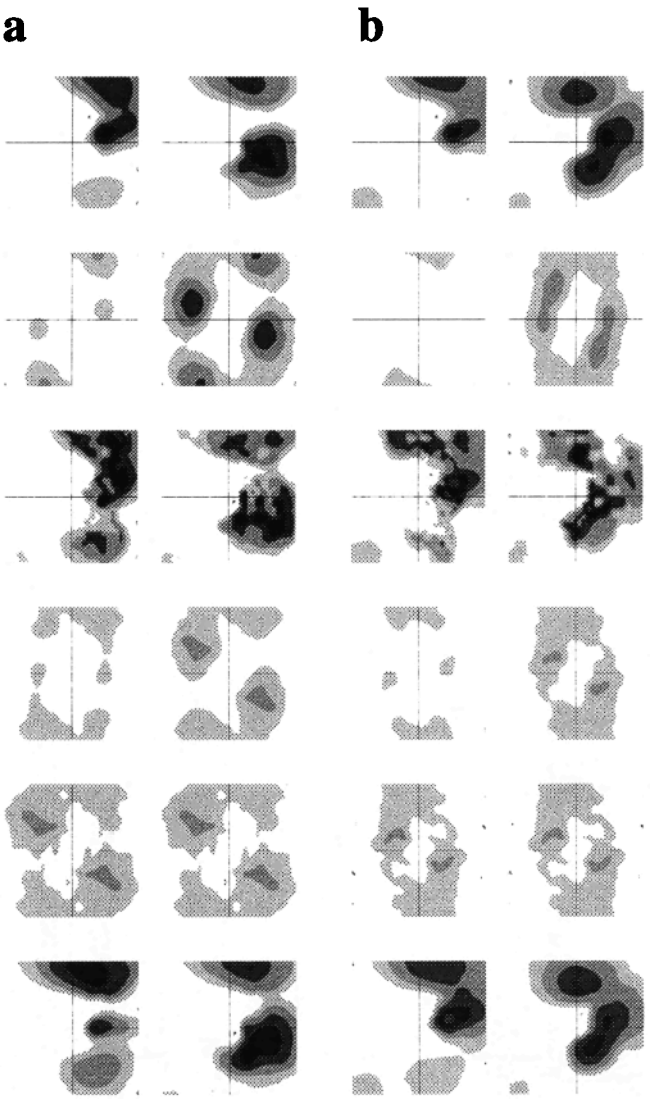

Figure 4. Retrieval of wave spectra from SAR image spectra observed at (a) 54.4 S, 33.6W and (b) 51S, 31.6W on January 30, 1993, 1139Z. Plots are in wavenumber space, k_x denotes azimuthal (flight) direction (197°). Column 1 is first iteration; column 2 is optimal iteration (Figure 4a, third iteration; Figure 4b fourth iteration). Row 1 is input wave spectrum, row 2 is SAR spectrum computed from input wave spectrum, row 3 is wave spectrum obtained from inversion of SAR spectrum, row 4 is simulated SAR spectrum, row 5 is observed SAR spectrum, and row 6 is retrieved wave spectrum.

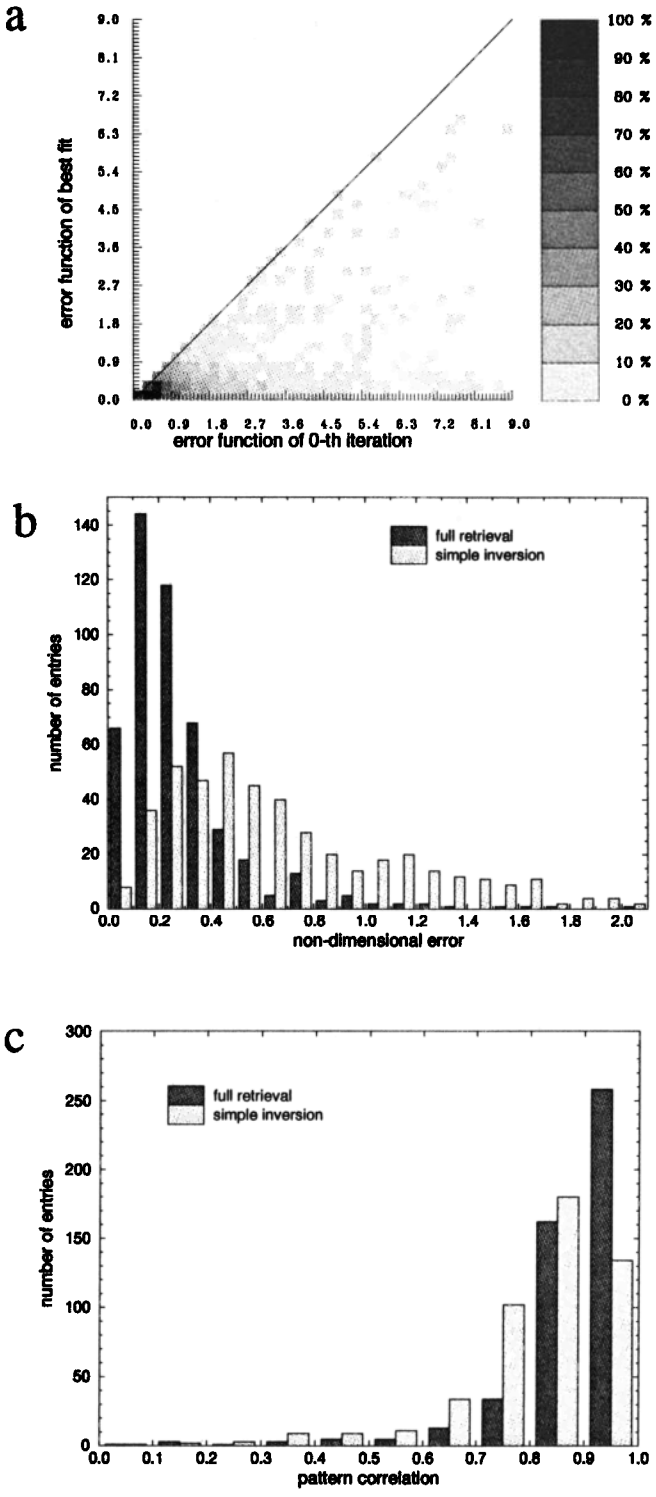

Figure 5. (a) Scatter diagram of errors between simulated and observed SAR spectra for noniterated and optimally iterated, minimal-error input spectra. Data represent 2729 spectra from March 8, 1993 to March 16, 1993. Grey scale represents density classes in increments of 10%, beginning with the lowest density (dark grey pixels, summing to 10% of all cases). (b) Distribution of the errors (equation (24)) between the ERS-1 SAR spectra and the SAR spectra computed from the iterated full retrievals (darker shaded columns) and from the single-shot retrievals (lighter shaded columns). (c) Same as Figure 5b for the spectral pattern correlations.

peak waves traveling northeastward but no system in the westerly direction. The latter can be clearly seen, however, in the first SAR inversion (Figure 7b) and is still more apparent in the final retrieved spectrum (Figure 7c, after two iterations). The pattern correlation index for the simulated and observed SAR spectrum increases from 0.61 for the simulated SAR spectrum of the zeroth iteration to 0.94 for the SAR spectrum computed from the optimally retrieved wave spectrum.

5. Conclusions and Outlook

The improved SAR retrieval algorithm features the following modifications of the original HH algorithm:

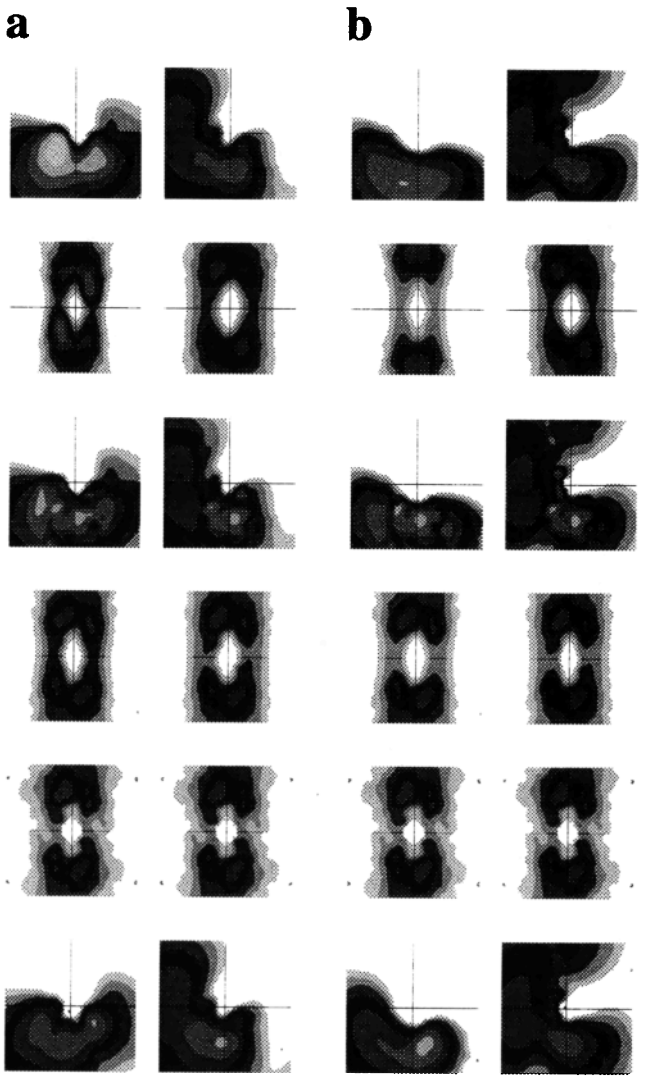

Figure 6. Retrieval of wave spectrum from SAR image spectrum at 57.7S, 19.0W, March 20, 1993, 0113Z using as first guess (a) a WAModel spectrum and (b) a Joint North Sea Wave Project (JONSWAP) spectrum. Plots are in wavenumber space; k_x denotes azimuthal (flight) direction (341° from north). Column 1 is first iteration, column 2 is last iteration. Row 1 is input wave spectrum, row 2 is SAR spectrum computed from input wave spectrum, row 3 is inverted SAR wave spectrum, row 4 is simulated SAR spectrum, row 5 is observed SAR spectrum, and row 6 is retrieved wave spectrum.

(1) An additional term in the cost function to enforce better agreement between the observed and simulated azimuthal cutoff, which leads to a change in the overall level of the wave spectrum, including the high wavenumber region not directly accessible to SAR observations; (2) the introduction of a smoothing procedure in computing the SAR spectrum from the inverted wave spectrum, thereby matching the SAR spectrum computations to the computations of the ERS-1 SAR wave mode fast delivery product; and (3) an additional iteration loop modifying the input wave spectrum, with the aid of a spectral partitioning technique, thereby allowing the retrieved wave spectrum to depart more strongly from the first-guess wave spectrum and achieve a closer agreement between the simulated and observed SAR spectrum.

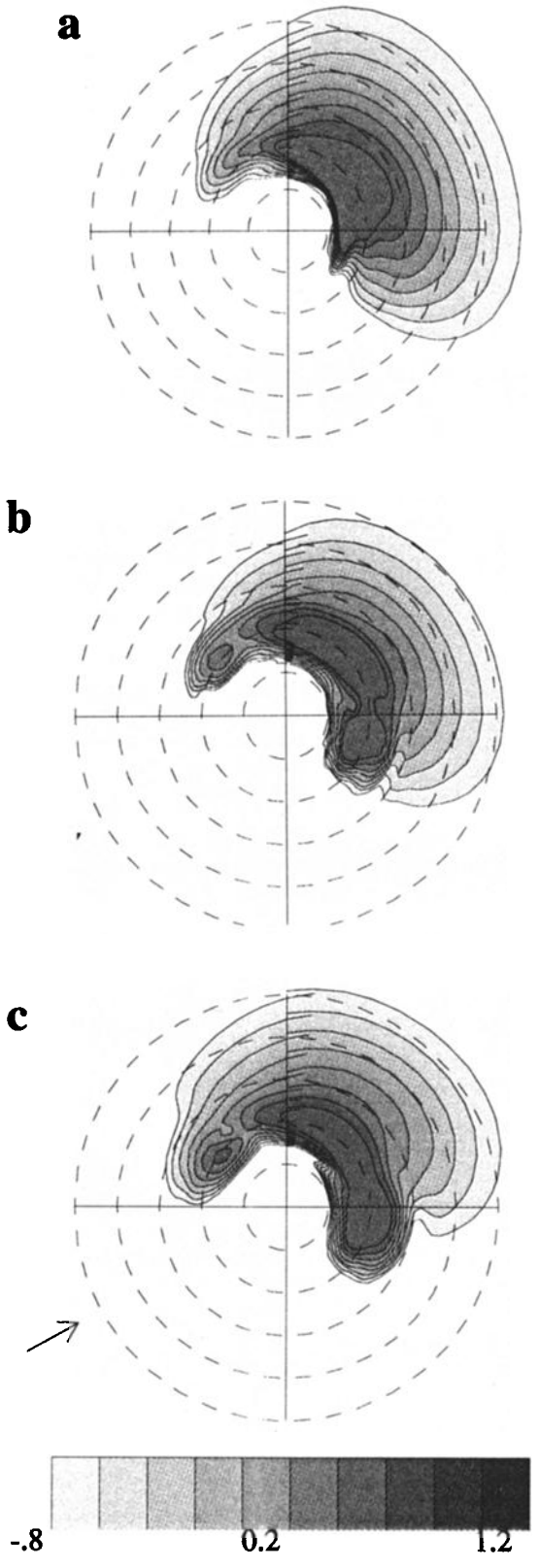

As mentioned in the introduction, the SAR imaging mechanism governing the mapping of a wave spectrum into a SAR image spectrum is well understood. The theoretical forward mapping relations have been validated by many comparisons of SAR observations with SAR spectra computed from buoy spectra and ship radar measurements. Residual discrepancies arising from the use of incorrect expressions for the modulation transfer functions in the forward mapping relation or SAR calibration errors have no impact, to first order, on the design of an optimal retrieval algorithm. The quality of a retrieval algorithm is determined simply by the ability to reproduce the observed SAR spectra from the retrieved wave spectra by applying the forward mapping relation. This feature is essentially independent of the modulation transfer functions used in the forward mapping relation or the accuracy of the SAR calibration. The high pattern correlations and low errors between SAR spectra computed from the retrieved wave spectra and the ERS-1 SAR observations indicate a significant improvement of the present retrieval algorithm compared with the original algorithm of HH.

A further advantage of the present scheme is that it yields as output not only the full two-dimensional wave spectrum but also the wave system parameters of the partitioned spectrum. This is useful for applications in wave data assimilation. The ERS-1 satellite yields about 1500 wave mode spectra daily. Without some form of data reduction, this represents an effectively unmanageable data set for operational data assimilation purposes. By reducing the number of parameters to the three characteristic parameters $(H_s, \bar{f}, \bar{\theta})$ of the individual wave systems of the partitioned spectrum, the present retrieval algorithm can be incorporated in wave data assimilation schemes currently under development (S. Hasselmann et al., submitted manuscript, 1996).

Figure 7. (a) First guess wave spectrum, (b) retrieval for the non-iterated first-guess input spectrum, and (c) the optimally iterated retrieved wave spectrum. Data were taken at 39N, 57W on January 30, 1993, 1436Z. Figure is a polar frequency-directional plot. Circles denote frequencies at 0.05-Hz intervals starting at 0.05 Hz.Isolines are logarithmically spaced relative to the maximum value of the spectral energy density.The arrow denotes speed (10m/sec) and direction of the local wind

More extensive statistical studies comparing three years of ERS-1 SAR retrievals with altimeter wave height observations from various satellites and two-dimensional spectral buoy observations are currently being carried out at the Max-Planck-Institut für Meteorologie and the Institut für Meereskunde der Universität Hamburg. Preliminary results indicate also an improved agreement between altimeter and SAR-retrieved wave heights using the present algorithm than for the previous inversion of HH.

We anticipate that the planned operational application of the present extended SAR retrieval algorithm to ERS SAR wave mode data will provide continuous, global wave spectral data for improved wind and wave analyses and forecasts. In addition, it will yield valuable data for the study of the detailed space-time dependent properties of two-dimensional wave spectra in the open ocean, thereby providing the basis for a better understanding of the physics of ocean waves and the improvement of third generation wave models.

Acknowledgments. The present work was supported by the Office of Naval Research under grant number N00014-92-J-1840 and N00014-94-1-0541 and by the Bundesministerium für Forschung und Technologie under grant number BMFT 50EE9413. The authors thank R. Brokopf (MPI) for providing the first-guess WAM spectra and ECMWF (Reading,England) for the wind analyses.

References

Alpers, W., and C. Brüning, On the relative importance of motion related contributions to the SAR imaging mechanism of ocean surface waves. *IEEE Trans. Geosci. Remote Sens., GE-24*, 873-885, 1986.

Alpers, W., and K. Hasselmann, Spectral signal-to-clutter and thermal noise properties of ocean wave imaging synthetic aperture radars. *Int. J. Remote Sens., 3*, 423-446, 1982.

Alpers, W., C. Brüning, and K. Richter, Comparison of simulated and measured synthetic aperture radar image spectra with buoy-derived ocean wave spectra during the Shuttle Image Radar B mission. *IEEE Trans. Geosci. Remote Sens., GE-24*, 559-566, 1986.

Bao, M., C. Brüning, and W. Alpers, A generalized nonlinear integral transform and its application to ERS-1 SAR ocean wave imaging, in *Space at the Service of our Environment, Proceedings of the Second ERS-1 Symposium, Hamburg, Germany, October 1993*, Eur. Space Agency Spec. Publ., *ESA SP - 361*, 219-224 1994.

Bauer, E., K. Hasselmann, I.R. Young, and S. Hasselmann, Assimilation of wave data into the wave model WAM using an impulse response function method. *J. Geophys. Res. 101*, 3801-3816, 1996.

Beal, R.C. (Ed.) Baltimore, Md., *Directional Ocean Wave Spectra*, pp. 117-124, Johns Hopkins Univ. Press, 1991.

Beal, R.C., D.G. Tilley, and F.M. Monaldo, Large- and small-scale spatial evolution of digitally processed ocean wave spectra from Seasat Synthetic Aperture Radar. *J. Geophys. Res., 88*, 1761-1778, 1983.

Brüning, C., W. Alpers, L.F. Zambresky, and D.G. Tilley, Validation of a SAR ocean wave imaging theory by the shuttle imaging radar-B experiment over the North Sea, *J. Geophys. Res., 93*, 15,403-15,425, 1988.

Brüning, C., W. Alpers, and K. Hasselmann, Monte Carlo simulation studies of the nonlinear imaging of a two-dimensional surface wave field by a synthetic radar, *Int. J. Remote Sens., 11*, 1695-1727, 1990.

Brüning, C., W. Alpers, and A. Wilde, Ocean Wave imaging by ERS-1 synthetic radar: First results from the Haltenbanken Calibration/Validation campaign, in *Proceedings of the ERS-1 Geophysical Validation Workshop, Penhors, Bretagne, France, 27-30 April 1992, Eur. Space Agency Spec. Publ., ESA WPP-36*, 169-177, 1992.

Brüning, C., S. Hasselmann, K. Hasselmann, S. Lehner, and T. Gerling, On the extraction of ocean wave height spectra from ERS-1 SAR wave model image spectra, in *Proceedings of the ERS-1 Workshop, Cannes, November, 1992, Eur. Space Agency Spec. Publ., ESA SP-359*, 747-752, 1993.

Brüning, C., S. Hasselmann, K. Hasselmann, S. Lehner, and T. Gerling, First evaluation of ERS-1 synthetic aperture radar wave mode data. *The Glob. Atmosph. and Ocean Syst., 2*, 61-98, 1994a.

Brüning, C., R. Schmidt, and W. Alpers, Estimation of the ocean wave radar modulation function from synthetic aperture radar imaging, *J. Geophys. Res., 99*, 9803-9816, 1994b.

Engen, G., H. Johnson, H.E. Krogstad, and S. Barstow, Directional wave spectra by inversion of ERS-1 synthetic aperture radar ocean imagery, *IEEE Trans. Geosci. and Remote Sens., 32, 2* 340-352, 1994.

Gerling, T.W., Partitioning sequences and arrays of directional wave spectra into component wave systems, *J. Atmos. Oceanic Technol., 9*, 444-458, 1992.

Hansen, B., C. Brüning, and C. Staabs, Global comparison of significant wave heights derived from ERS-1 SAR wave mode, ERS-1 altimeter and TOPEX altimeter data, in *Space at the Service of our Environment, Proceedings of the Second ERS-1 Symposium, Hamburg, Germany, October 1993, Euro. Space Agency Spec. Publ., ESA SP - 361*, 33-36, 1994.

Hasselmann, K. and S. Hasselmann, On the nonlinear mapping of an ocean wave spectrum into a SAR image spectrum and its inversion, *J. Geophys. Res., 96*, 10,713-10,729, 1991.

Hasselmann, K., et al., Measurements of wind-wave growth and swell decay during the Joint North Sea Wave Project (JONSWAP), *Dtsch. Hydrogr. Z. Suppl. A, 8* (12), 95pp, 1973.

Hasselmann, K., R.K. Raney, W.J. Plant, W. Alpers, R.A. Shuchman, D.R. Lyzenga, C.L. Rufenach and M.J. Tucker, Theory of synthetic aperture radar ocean imaging; A MARSEN view, *J. Geophys. Res., 90*, 4659-4686, 1985.

Hasselmann, K., S. Hasselmann, E. Bauer, C. Brüning, S. Lehner, H. Graber, and P. Lionello, Development of a satellite SAR image spectra and altimeter wave height data assimilation system for ERS-1. *ESA Report, 19, Max-Planck-Institute für Meteorologie*, Hamburg, Germany, 1988.

Hasselmann, K., S. Hasselmann, C. Brüning, and A. Speidel, Interpretation and application of SAR wave image spectra in wave models, in *Directional Ocean Wave Spectra*, edited by R.C. Beal, pp. 117-124, Johns Hopkins Univ. Press, Baltimore, Md., 1991.

Hasselmann, S., K. Hasselmann, and C. Brüning, Extraction of wave spectra from SAR image spectra, in *Dynamics and Modelling of Ocean Waves*, edited by G. Komen, pp. 391-401, Cambridge Univ. Press, Cambridge, England, 1994a.

Hasselmann, S., C. Brüning, and P. Lionello, Towards a generalized optimal interpolation method for the assimilation

of ERS-1 SAR retrieved wave spectra in a wave model, in *Space at the Service of our Environment, Proceedings of the Second ERS-1 Symposium, Hamburg, Germany, October, 1993, Eur. Space Agency Spec. Publ., ESA SP - 361*, 21-25, 1994b.

Hasselmann, S., et al., Assimilation of wave observations, in *Dynamics and Modelling of Ocean Waves*, edited by G. Komen, 405-480, Cambridge University Press, Cambridge, England, 1994c.

Komen, G., L. Cavaleri, M. Donelan, K. Hasselmann, S. Hasselmann, and P.A.E.M. Janssen, *Dynamics and Modelling of Ocean Waves*, Cambridge University Press, Cambridge, England, 1994.

Krogstad, H.E., A simple derivation of Hasselmann's nonlinear ocean-synthetic aperture radar transformation, *J. Geophys. Res, 97*, 2421-2425, 1992.

Plant, W.J. and W. Alpers, An introduction to SAXON-FPN, *J. Geophys. Res., 99*, 9699-9703, 1994.

Wave Model Development and Implementation (WAMDI) Group, The WAM model - A third generation ocean wave prediction model. *J. Phys. Oceanogr., 18*, 1775-1810, 1988.

Wilde A., C. Brüning, W. Alpers, V. Etkin, K. Litovchenko, A. Ivanov, and V. Zajtsev, Comparison of ocean wave imaging by ERS-1 and ALMAZ-1 synthetic aperture radar, in *Space at the Service of our Environment, Proceedings of the Second ERS-1 Symposium, Hamburg, Germany, October 1993, Euro. Space Agency Spec. Publ., ESA SP - 361*, 239-245, 1994.

Young, I.R., S. Hasselmann, and K. Hasselmann, Computations of the response of a wave spectrum to sudden changes in the wind direction. *J. Phys. Oceanogr., 17*, 1317-1318, 1987.

C. Brüning, European Commission, Directorate-General for Science, Research and Development, Brussels, Belgium. (e - mail: claus.bruning@dg12.cec.be)

K. Hasselmann, S. Hasselmann, and P. Heimbach, Max-Planck-Institut für Meteorologie, Bundesstraße 55, 20146 Hamburg, Germany. (e-mail: klaus.hasselmann@dkrz.de; susanne.hasselmann@dkrz.de, heimbach@dkrz.de

(Received April 7, 1995; revised December 18, 1995; accepted February 26, 1996.)